Supplementary Materials for

How Far can Nature-Based Solutions Increase Water Supply Resilience to Climate Change in One of the Most Important Brazilian Watersheds?

1. SWAT model operation description

The SWAT model operates dividing the simulations into land phase (models the amount of water, sediments, nutrients, and pesticides carried from subbasins to their respective main channels) and routing phase (which represents how these loads flow through the drainage network to the watershed outlet). The water balance equation governs the processes simulated in the land phase [1].

The model divides the watershed into subbasins and further divides the subbasins into smaller units that correspond to unique combinations of land use, soil type, and slope class, known as Hydrologic Response Units (HRUs) [1]. The outputs are generated for each HRU and then grouped for each subbasin. To delimit the Atibainha river basin, automatic watershed delineation based on DEM was used. In total, 10 subbasins and 880 HRUs were created. To create HRUs representative of all the variability present in the basin, no threshold of minimum area of occurrence for soil, land use, or slope class, was determined.

2. Model setup

2.1. Baseline model

Topography was divided in five slope classes that had a similar occurrence in the watershed: 0-5% (21.6%), 5-15% (13.3%), 15-25% (15.2%), 25-45 (24.3%) and >45% (25.6%).

The land use map was manually reviewed and updated using OrbView and WorldView satellite images (years 2011 and 2012) to more accurately delimit the location of built-up areas and roads. The land use map selected, despite having been developed with less recent images, has a greater spatial resolution and level of detail in contrast to other maps available for the watershed. To assess whether the land use map, created with 2011 satellite images, was still consistent with the present reality of the basin, 603 random points were created according to Lillesand, Kiefer, and Chipman's [2] recommendations to evaluate a minimum of 50 points per use class. At those points, the use class assigned by the map was contrasted manually with Vivid satellite images for the year 2019. A confusion matrix was generated and the Kappa value was calculated (Table S1). General accuracy obtained was high (94.5%) and Kappa accuracy index (0.93) was classified as excellent [3], indicating that the map chosen is suitable for creating a current model of the Atibainha river basin.

Table S1. Confusion matrix used to assess the accuracy of the land use map.

Land Use Land Cover Class*	WATR	EUCA	FRSE	PAST	UTRN	URLD	Total	Accuracy (U)	Kappa
WATR	50	0	0	0	0	0	50	1	
EUCA	0	121	3	2	0	0	126	0.96	
FRSE	1	2	189	0	0	1	192	0.984	
PAST	0	20	3	111	0	0	135	0.822	
UTRN	0	0	0	0	50	0	50	1	
URLD	0	0	0	0	1	49	50	0.98	
Total	51	143	195	113	51	50	603	-	
Accuracy (P)	0.98	0.85	0.97	0.982	0.98	0.98	-	0.945	
Kappa									0.93

*Land use codes applied in the table are the same for SWAT database: EUCA = Eucalyptus; FRSE = Forest-Evergreen; PAST = Pasture; URLD = Residential low-density; UTRN = Urban transportation; WATR = Water.

The soil map has been updated through a new photointerpretation of the relationship between soil and landscape, increasing compatibility between the landforms and the soil classes indicated. The update allowed the separation of soil type associations present in the original map and the inclusion of other soil classes with a high probability of occurrence in the study area.

All meteorological and rain stations near the study site were compiled and tested in different combinations of weather data sets (Table S2). The data sets effects on the uncalibrated model performance were evaluated by comparing the simulated and observed streamflow in 2 river gauges selected for the model calibration, using commonly applied hydrologic model performance statistics (Nash-Sutcliffe efficiency coefficient (NS), Percent bias (PBIAS), and the coefficient of determination (R^2)). The best results were obtained when using daily measured temperature and precipitation data from 2009 to 2019, obtained from one meteorological station near the basin outlet, and SWAT's weather generator to fill the gaps in the data time series.

Table S2. Sources of climate data and weather data set combinations analyzed. IAC corresponds to the Agronomic Institute of Campinas; DAEE corresponds to Water and Electric Energy Department; Sabesp is the Basic Sanitation Company of São Paulo State; WGEN corresponds to SWAT's Weather Generator and INMET is the National Meteorology Institute.

Combination id	Precipitation source	Temperature source	Remaining climate parameters*
1	IAC	IAC	WGEN
2	IAC + Hidroweb + DAEE + Sabesp	IAC	WGEN
3	IAC + Hidroweb + DAEE + Sabesp (only stations with at least 85% of time series complete)	IAC	WGEN

4	IAC + Hidroweb + DAEE + Sabesp (Gaps in time series manually filled with data from nearby stations)	IAC	WGEN
5	IAC + Hidroweb + DAEE + Sabesp (only stations with at least 85% of time series complete and gaps in time series manually filled with data from nearby stations)	IAC	WGEN
6	IAC	IAC (Gaps in time series manually filled with data from nearby stations)	WGEN
7	IAC	IAC (Gaps in time series manually filled with data from nearby stations)	INMET
8	IAC	IAC	INMET
9	WGEN	WGEN	WGEN
10	IAC	WGEN	WGEN

* Remaining parameters correspond to wind speed, solar radiation, and relative humidity.

Regional studies supported the alteration of SWAT database default values for some key parameters aiming to represent more accurately the study area condition. The altered parameters were: plant growth factors (Table S3); initial plant growth parameters for vegetation that doesn't require a "plant/begin growing" operation since they are already growing at the beginning of the simulation (Table S4); C-factor (Table S5); and curve-number (Table S6).

Table S3. Plant growth factors altered according to regional studies. Vegetation type corresponds to SWAT land use codes: EUCA = Eucalyptus, FRSE = Forest-Evergreen and PAST = Pasture.

Parameter	Description	Vegetation type	Original value	Altered value	Source
BLAI	Maximum potential leaf area index (m^2/m^2)	EUCA	2.5	3.5	[4]
		FRSE	5	7	[5]
		PAST	4	3.2	[6]
ALAI_MIN		EUCA	0.75	2.2	[4]

	Minimum leaf area index during dormancy (m^2/m^2)	FRSE	0.75	6	[5]
		PAST	0	1.6	[6]
CHTMX	Maximum canopy height (m)	EUCA	3.5	21	[7]
		FRSE	10	10	[8]
		PAST	0.5	0.3	[9]
BIO_LEAF	Fraction of tree biomass accumulated each year that is converted to reside during dormancy	EUCA	0.3	0.3	Default value
		FRSE	0.3	0.015	Manual adjust
		PAST	0	0	Default value
BM_DIEOFF	Biomass fraction that dies during dormancy	EUCA	0.1	0.1	Default value
		FRSE	0.1	0.04	Manual adjust
		PAST	0.1	0.04	Manual adjust

Table S4. Initial plant growth parameters altered according to regional studies. Vegetation type corresponds to SWAT land use codes: EUCA = Eucalyptus, FRSE = Forest-Evergreen and PAST = Pasture.

Parameter	Description	Vegetation type	Value	Source
LAI_INIT	Initial leaf area index (m^2/m^2)	FRSE	7	[5]
		PAST	3,2	[6]
BIO_INIT	Initial dry weight biomass (kg/ha)	FRSE	150,000	[10]
		PAST	1,500	[11]
PHU_PLT	A total number of heat units or growing degree days needed to bring plant to maturity.	FRSE	8,000	Manual adjustment
		PAST	3,500	[12]

Table S5. Universal Soil Loss Equation C factor altered according to regional studies. Vegetation type corresponds to SWAT land use codes: EUCA = Eucalyptus, FRSE = Forest-Evergreen and PAST = Pasture.

Vegetation type	C-factor	Source
EUCA	0.05	[13]
FRSE	0.003	[13]
PAST	0.03	[14]

Table S6. Universal Soil Loss Equation C factor altered according to regional studies. Vegetation type corresponds to SWAT land use codes: EUCA = Eucalyptus, FRSE = Forest-Evergreen and PAST = Pasture. Here are also shown curve numbers used for the two new land use classes added to the SWAT database to represent the condition of managed eucalyptus (RFLO) and pasture uses (PMAN).

Vegetation type	Curve number* for each soil's hydrologic group and each land use-land cover			
	A	B	C	D
EUCA	45	66	77	83
RFLO	35	55	70	70
FRSE	20	40	49	52
PAST	49	69	79	84
PMAN	39	61	74	80

*Curve number values extracted from Sartori, [15].

2.2. Land use-land cover change scenarios

To build the land use map for the riparian conservation scenario, the hydric Permanent Preservation Areas (APP) layer for the basin was obtained from the Brazilian Foundation for Sustainable Development (FBDS) [4] and joined with the current land use map. Impervious areas located inside the APPs limits were maintained, given that to implement this strategy, buildings and roads wouldn't be modified.

To build the land use map for the focal conservation scenario, the first step was to apply the Conservative Use Potential (PUC) method. The lithology map for São Paulo state [5] was applied with the current scenario' DEM and soil map to determine the watershed's PUC classes. In the following step, the PUC raster produced was overlayed with the current land use map. All sites containing eucalyptus plantations and pastures in areas with classes equal to 4 or 5 had their SWAT land use code modified from EUCA (eucalyptus) and PAST (pasture) to RFLO (reforestation) and PMAN (managed pasture), respectively.

The codes RFLO and PMAN represent two new land use classes added to the SWAT database to represent a condition of managed eucalyptus and pasture uses, respectively. For both new land uses, the curve number was altered to represent best management practices (Table S6). Additionally, to represent pasture best management practices the following parameters were also modified based on literature values: C-factor value; maximum and minimum leaf area index; maximum canopy water storage; initial leaf area index; and initial dry weight biomass (Table S7).

Table S7. Parameters altered to represent best management practices adopted in pasture areas in land use scenarios focal conservation and combined solutions.

Parameter	Description	Value	Source
C-factor	Minimum value of USLE C factor for water erosion applicable to the land cover/plant	0.008	[14]
BLAI	Maximum potential leaf area index (m^2/m^2)	3.6	[9]
ALAI_MIN	Minimum leaf area index during dormancy (m^2/m^2)	3.2	[9]
CANMX	Maximum canopy storage (mm H_2O)	1.33	[16]
LAI_INIT	Initial leaf area index (m^2/m^2)	3.6	[9]
BIO_INIT	Initial dry weight biomass (kg/ha)	2.700	[16]

2.3. Land use-land cover change scenarios results

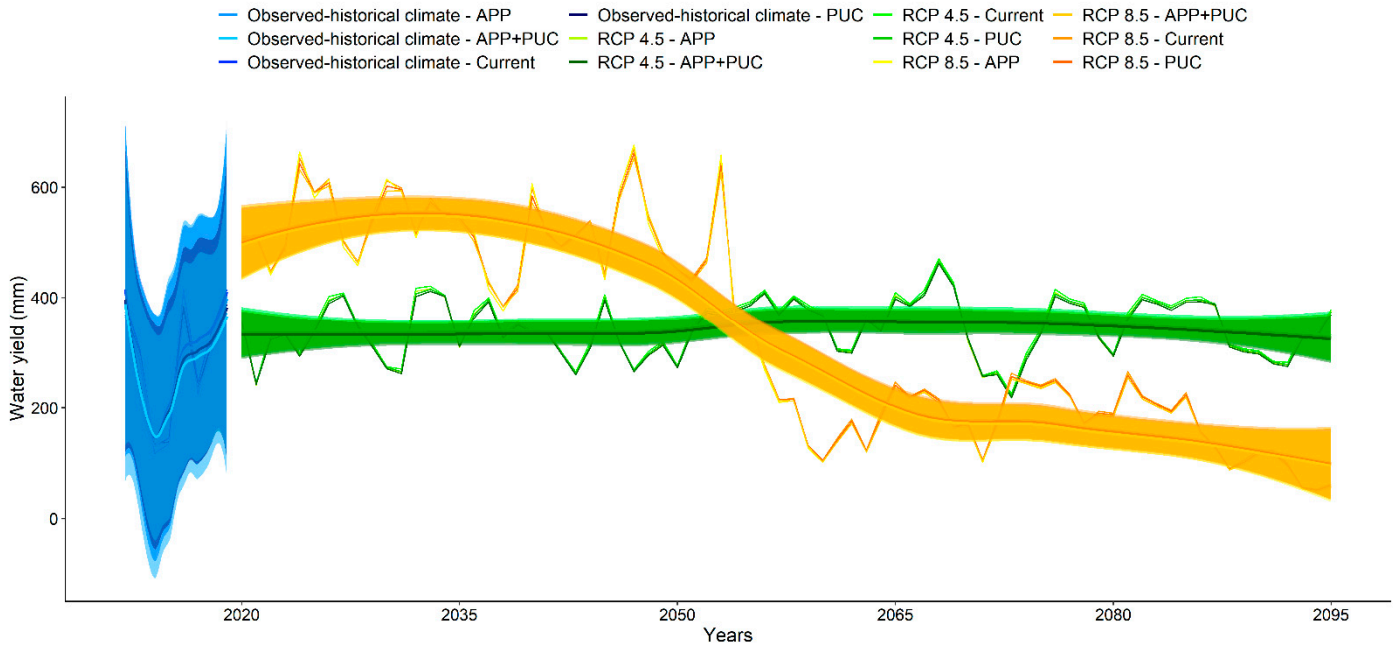

Figure S1. Annual mean water yield for each climate condition (observed-historical, RCP 4.5 and RCP 8.5) and each LULC scenario (Current, APP = riparian restoration, PUC = focal conservation and APP+PUC = combined solutions). Shaded area shows the 95% confidence interval.

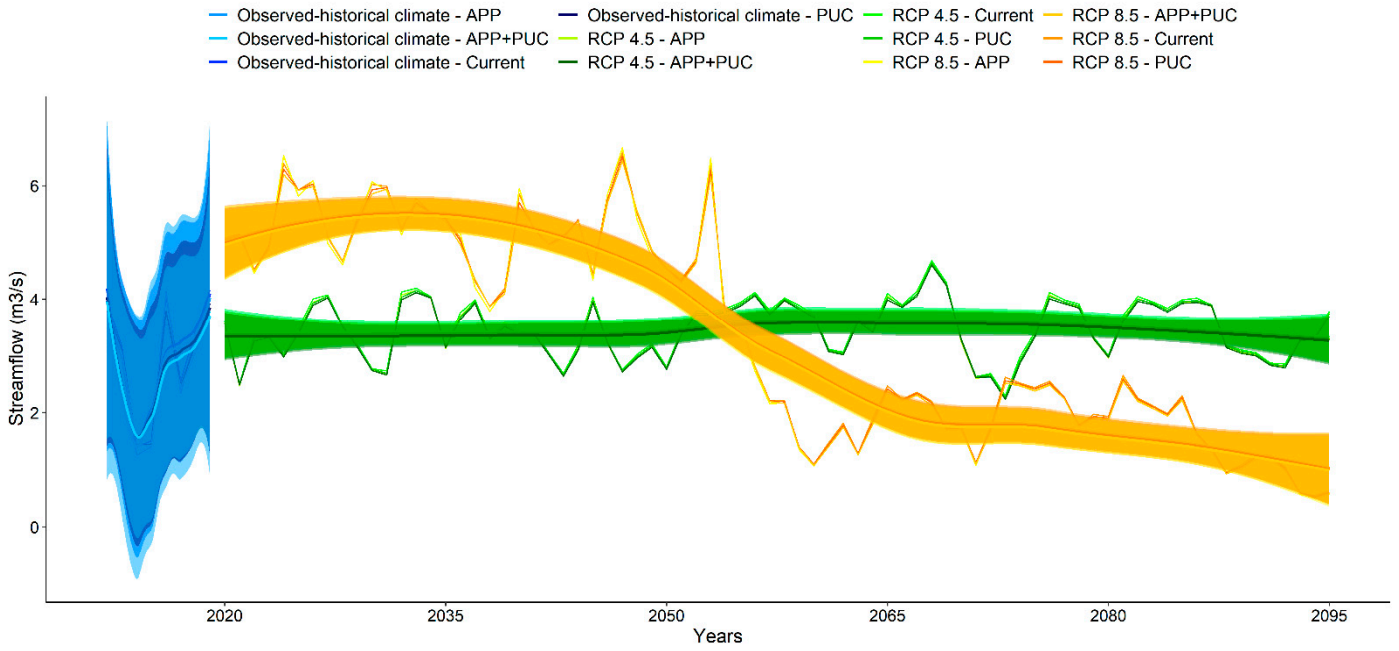

Figure S2. Annual mean streamflow into the basin's outlet reach for each climate condition (observed-historical, RCP 4.5 and RCP 8.5) and each LULC scenario (Current, APP = riparian restoration, PUC = focal conservation and APP+PUC = combined solutions). Shaded area shows the 95% confidence interval.

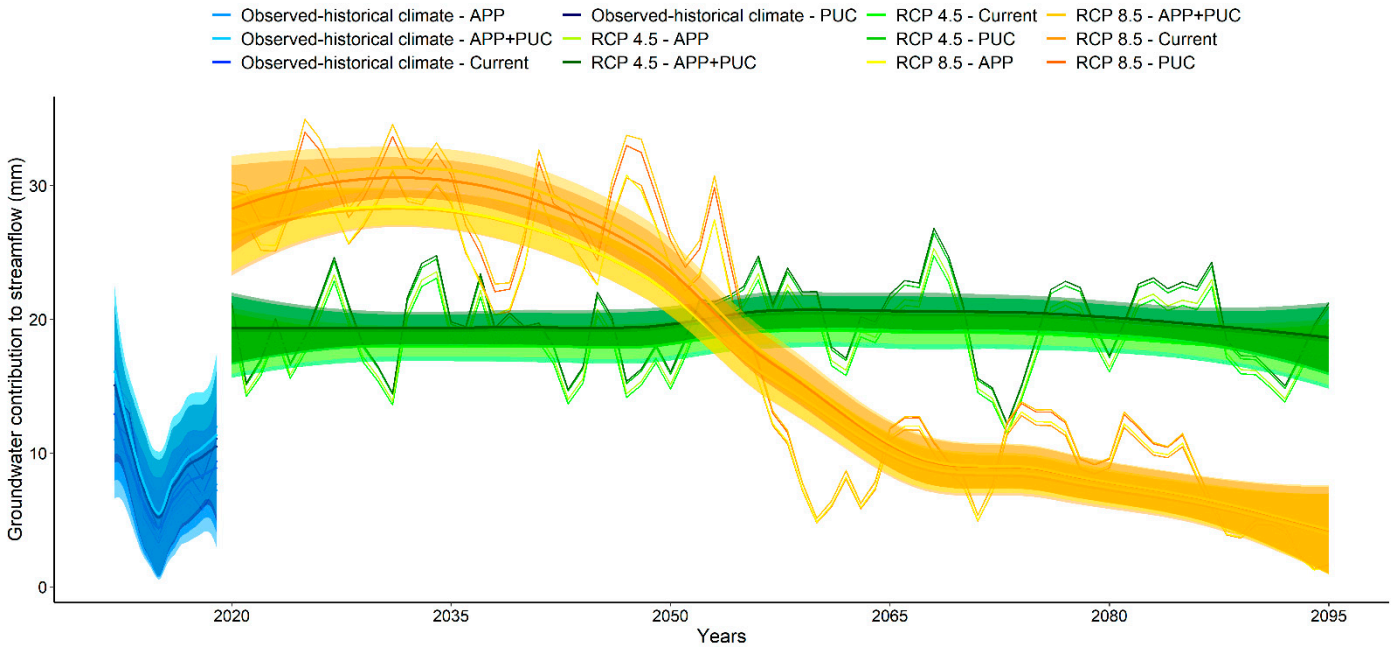

Figure S3. Annual mean groundwater contribution to streamflow for each climate condition (observed-historical, RCP 4.5 and RCP 8.5) and each LULC scenario (Current, APP = riparian restoration, PUC = focal conservation and APP+PUC = combined solutions). Shaded area shows the 95% confidence interval.

2.4. Climate change scenarios

The NASA Earth Exchange Global Daily Downscaled Projections (NEX-GDDP) dataset was downloaded from the NASA data portal available at https://nex.nasa.gov/nex/static/htdocs/site/extra/opennex/. The mean multi-model ensemble approach was used to represent the climate change scenarios (Table S8). The multi-model ensemble approach combines different weather forecasts obtained by different climate models that are run with slight differences towards their initial conditions, in order to account for the uncertainty of those conditions [17]. The use of the multi-model ensemble approach has been recommended in hydrologic studies because its predictions are generally considered superior compared to single projection data. Moreover, multi model ensembles are commonly used to reduce the uncertainties of future climate estimates [18,19].

Quantile mapping was used for bias correction in the daily precipitation data. quantile mapping, a widely used and robust methodology for bias correction of daily precipitation data [20]. We emphasize that due to the unavailability of historical maximum and minimum temperature data, bias correction on this variable was not possible.

Table S8. List of NEX-GDDP models used for the mean multi-model ensemble.

Model	Country	RCP 4.5	RCP 8.5
ACCESS1.0	Australia	X	X
BCC-CSM1.1	China	X	X
CNRM-CM5	France	X	X
CSIRO-MK3.6.0	Australia	X	X
GDFL-CM3	United States	X	X
GDFL-ESM2G	United States	X	X
GDFL-ESM2M	United States	X	X
INM-CM4	Russia	X	X
IPSL-CM5A-MR	France	X	X
MIROC-ESM	Japan	X	X
MIROC-ESM-CHEM	Japan	X	X
MPI-ESM-LR	Germany	X	X
MPI-ESM-MR	Germany	X	X
MRI-CGCM3	Japan	X	X
NORESM1-M	Norway	X	X

3. Model calibration and validation

3.1. Calibration and validation procedures

Each gauge was calibrated separately, starting with the one located upstream and following to the other downstream. Calibrated values of parameters were substituted and fixed for one gauge and its tributaries before moving to the next [21]. The first three years of the time series were used as model warm-up period. The remaining years were equally split between calibration and validation and the group of years applied in each of these procedures at each station, was selected in order to ensure that the mean and variance of discharges presented values as close as possible for both periods [22] (Table S9).

Table S9. Streamflow stations and periods used for calibration and validation.

Streamflow Gauges	Station Code	Source	Sub-basin	Time Series	Calibration	Validation
Nazaré Paulista	62655800	National Water Agency (ANA)	7	July 2014 – December 2019	2015, 2017 and 2019	2014, 2016 and 2018
Barragem Afluente	62653510	Basic Sanitation Company of São Paulo State (SABESP)	5 (Watershed outlet)	January 2009 – December 2019	2012 – 2014 and 2019	2015 - 2018

Calibration and validation were performed semi-automatically in the SWAT-CUP program [23] using the SUFI-2 (Sequential Uncertainty Fitting) optimization algorithm [24] and Kling-Gupta Efficiency (KGE) as goal function [25]. In SUFI-2 the uncertainty present in the inputs and outputs is taken into account, quantified, and represented by the 95% prediction uncertainty (95PPU). The strength of a given calibration is linked to the percentage of observations contained within the 95PPU band (indicated by the P-factor statistic) and the average width of that band (indicated by the R-factor statistic) [24]. For discharge calibration, satisfactory P-factor and R-factor are more than 70% and closer to 1, respectively. KGE values range from 0 to 1, values greater or equal to 0.5 are considered satisfactory results [26]. The best calibration solution was considered the one that resulted in the best set of values for KGE, P-factor, and R-factor statistics. Results are also shown for Nash-Sutcliffe (NS; [27]), Percent Bias (PBIAS), and the coefficient of determination (R^2) performance statistics.

The canopy maximum water storage (CANMX) parameter had its range values determined according to literature measured values for each vegetation type present in the basin: eucalyptus [28,29], forest [30,31], and pasture [29,16]. This parameter introduces water in the system and thus was fitted first, separately from the others, had its best values fixed, and was removed from the calibration prior to adjustments in further inputs, following Abbaspour and colleagues' recommendation [22]. This was done through the execution of 1 iteration made of 100 simulations. The next step was to run an iteration with 500 simulations and perform a global sensitivity analysis [23] for 17 parameters related to streamflow and selected from the literature [21,24,1,32]. Only the most sensitive inputs for each station were included in the following iterations. Iterations were made until the best set of values for the aforementioned statistics was obtained. Parameter sensitivities, calibrated ranges, and adjusted values can be found in Tables S10 and S11, respectively.

Table S10. More sensitive parameters according to global sensitivity analysis for each streamflow gauge.

Streamflow gauge	Parameter	t-Stat	p-value
Nazaré Paulista	v_EPCO.hru	20.13	0.000000000
	r_SOL_BD().sol	-17.07	0.000000000
	r_SOL_K().sol	-14.73	0.000000000
	r_SOL_AWC().sol	14.22	0.000000000
	v_ESCO.hru	-7.09	0.000000000
	r_SLSUBBSN.hr	4.51	0.000008058
	v_GW_DELAY.gw	-3.00	0.0000038012
Barragem Afluente	v_RCHRG_DP.gw	14.66	0.000000000
	v_GW_DELAY.gw	9.49	0.000000000
	v_EPCO.hru	5.20	0.000000303

Table S11. Parameters used for calibrating the base model, original values, modification range applied and final fitted value, and respective sub-basin of application.

Parameter	Subbasins	Original value	Modification range	Fitted value
v_CANMX.hru_EUCA	1-10	0	0 to 2.5	2.1625
v_CANMX.hru_FRSE	1-10	0	0 to 8	7.88
v_CANMX.hru_PAST	1-10	0	0 to1	0.665
r_CN2.mgt*	1-6, 8-10 7	Variable	-0.1 to 0.1	-0.0738 -0.0894
r_CN2.mgt**	1-6, 8-10 7	Variable	-0.1 to 0.1	0.053 -0.0634
r_SOL_AWC().sol	1-6, 8-10 7	Variable	-0.25 to 0.27	-0.01132 0.11452
r_SOL_K().sol	1-6, 8-10 7	Variable	-0.25 to 0.25	-0.2335 -0.1925
r_SOL_ALB().sol	1-6, 8-10 7	Variable	-0.25 to 0.1	-0.0515 -0.11735
r_SOL_BD().sol	1-6, 8-10 7	Variable	-0.3 to 0.015	-0.044535 -0.223455
v_GWQMN.g	1-6, 8-10 7	1000	0 to 2000	334 1542
v_GW_REVAP.gw	1-6, 8-10 7	0.02	0.02 to 0.2	0.1847 0.16346
v_GW_DELAY.gw	1-6, 8-10 7	31	0 to 500	454.5 25.5
v_RCHRG_DP.gw	1-6, 8-10 7	0.05	0 to 1	0.903 0.923
v_REVAPMN.gw	1-6, 8-10 7	750	0 to 1000	753 463
v_ALPHA_BF.gw	1-6, 8-10 7	0.048	0 to 1	0.023 0.373
v_EPCO.hru	1-6, 8-10 7	1	0 to 1	0.839 0.917
v_ESCO.hru	1-6, 8-10 7	0.95	0.6 to 1	0.9124 0.7476
r_SLSUBBSN.hru	1-6, 8-10 7	Variable	-0.15 to 0.23	0.1217 0.22506
v_CH_K2.rte	1-6, 8-10 7	0	0.025 to 25	10.089925 17.782225
v_CH_N2.rte	1-6, 8-10 7	0.014	0 to 0.15	0.11235 0.08265

*CN2 calibrated separately for the uses of eucalyptus and pasture present in soils of hydrological group A. **CN2 calibrated separately for all uses present in soils of hydrological groups C and D. The table shows the original values of the parameters (present in the default model), the range of values for the parameter for calculating the 95PPU band, and the final calibrated values. The r operator corresponds to the relative method for changing values, where the current value is multiplied by 1 + x, with x being a value within the defined maximum and minimum limits. v corresponds to the substitution method, where the parameter value is replaced by another value within the defined limits. The file to which each parameter belongs is indicated by the extension present in its definition (e.g.: .mgt the file of inputs of handling parameters).

3.2. Calibration and validation results

The results of the calibration of the base model in sub-basin 7 were considered satisfactory for all evaluated statistics, with the exception of NS, according to the performance ratings proposed by Moriasi and colleagues [33] and by Kouchi et. al. [26] for monthly time step (Table S12). The validation in sub-basin 7, however, presented worse results, being considered adequate only according to PBIAS. Nevertheless, both the calibration and the validation of the base model at the basin outlet showed good results, having obtained satisfactory values for all performance metrics (with the exception of NS value for validation), as well as an excellent coverage of measured streamflow by the final calibration ranges (P-factor ≥ 70%) and a low uncertainty (R-factor < 1).

Table S12. Performance statistics of base model calibration and validation for monthly streamflow.

Streamflow Gauges	Period	P-factor	R-factor	KGE	NS	PBIAS	R^2
Nazaré Paulista	Calibration	0.37	0.73	0.72	0.5	9.8	0.65
	Validation	0.42	1.21	0.37	-0.5	20	0.37
Barragem Afluente	Calibration	0.71	0.83	0.83	0.67	3.9	0.72
	Validation	0.69	0.99	0.71	0.42	10.5	0.59

References

1. Arnold, J.G.; Moriasi, D.N.; Gassman, P.W.; Abbaspour, K.C.; White, M.J.; Srinivasan, R.; Santhi, C.; Harmel, R.D.; Van Griensven, A.; Van Liew, M.W. SWAT: Model Use, Calibration, and Validation. *Trans. ASABE* **2012**, *55*, 1491–1508. https://doi.org/10.13031/2013.42256.
2. Lillesand, T.; Kiefer, R.W.; Chipman, J. *Remote Sensing and Image Interpretation*; John Wiley & Sons: Hoboken, NJ, USA, 2015; ISBN 978-1-118-34328-9.
3. Landis, J.R.; Koch, G.G. The Measurement of Observer Agreement for Categorical Data. *Biometrics* **1977**, *33*, 159–174. https://doi.org/10.2307/2529310.
4. Hubbard, R.M.; Stape, J.; Ryan, M.G.; Almeida, A.C.; Rojas, J. Effects of Irrigation on Water Use and Water Use Efficiency in Two Fast Growing Eucalyptus Plantations. *For. Ecol. Manag.* **2010**, *259*, 1714–1721. https://doi.org/10.1016/j.foreco.2009.10.028.
5. de Almeida, A.C.; Soares, J.V. Comparação Entre Uso de Água Em Plantações de Eucalyptus Grandis e Floresta Ombrófila Densa (Mata Atlântica) Na Costa Leste Do Brasil. *Rev. Árvore* **2003**, *27*, 159–170.
6. Roberts, J.; Cabral, O.M.R.; da Costa, J.P.; McWilliam, A.L.C.; Sá, T.d.A. Plant Physiological Studies in Tropical Rainforest and Pasture in Amazonia. In *Embrapa Amazônia Ocidental-Artigo em Anais de Congresso (ALICE), Proceedings of the Congresso Brasileiro de Fisiologia Vegetal, Lavras, Brazil, 5, 1995*; Federal University of Lavras-UFLA: Lavras, Brazil, 1995.
7. Cabral, O.M.R.; Rocha, H.R.; Gash, J.H.C.; Ligo, M.A.V.; Freitas, H.C.; Tatsch, J.D. The Energy and Water Balance of a Eucalyptus Plantation in Southeast Brazil. *J. Hydrol.* **2010**, *388*, 208–216. https://doi.org/10.1016/j.jhydrol.2010.04.041.
8. Ditt, E.H.; Knight, J.D.; Mourato, S.; Padua, C.V.; Martins, R.R.; Ghazoul, J. Defying Legal Protection of Atlantic Forest in the Transforming Landscape around the Atibainha Reservoir, South-Eastern Brazil. *Landsc. Urban Plan.* **2008**, *86*, 276–283. https://doi.org/10.1016/j.landurbplan.2008.04.001.
9. Lara, M.A.S.; Silva, V.J.; Sollenberger, L.E.; Pedreira, C.G.S. Seasonal Herbage Accumulation and Canopy Characteristics of Novel and Standard Brachiariagrasses under N Fertilization and Irrigation in Southeastern Brazil. *Crop Sci.* **2021**, *61*, 1468–1477. https://doi.org/10.1002/csc2.20353.
10. Ditt, E.H.; Mourato, S.; Ghazoul, J.; Knight, J. Forest Conversion and Provision of Ecosystem Services in the Brazilian Atlantic Forest. *Land Degrad. Dev.* **2010**, *21*, 591–603. https://doi.org/10.1002/ldr.1010.
11. Uezu, A.; Sarcinelli, O.; Chiodi, R.; Jenkins, C.N.; Martins, C.S. *Atlas dos Serviços Ambientais do Sistema Cantareira*, 1st ed.; IPÊ-Instituto de Pesquisas Ecológicas: Nazaré Paulista, Brazil, 2017; ISBN 978-85-7954-113-1.
12. Marhaento, H.; Booij, M.J.; Rientjes, T.; Hoekstra, A.Y. Attribution of Changes in the Water Balance of a Tropical Catchment to Land Use Change Using the SWAT Model. *Hydrol. Process.* **2017**, *31*, 2029–2040. https://doi.org/10.1002/hyp.11167.
13. da Cunha, E.R.; Bacani, V.M.; Panachuki, E. Modeling Soil Erosion Using RUSLE and GIS in a Watershed Occupied by Rural Settlement in the Brazilian Cerrado. *Nat. Hazards* **2017**, *85*, 851–868. https://doi.org/10.1007/s11069-016-2607-3.
14. Vázquez-Fernández, G.Á.; Formaggio, A.R.; Epiphanio, J.C.N.; Gleriani, J.M. Determinação de Sequências Culturais em Microbacia Hidrográfica para Caracterização do Fator C da EUPS, Utilizando Fotografia Aérea. In Proceedings of the Anais VIII Simpósio Brasileiro de Sensoriamento Remoto, Salvador, Brasil, 14–19 April 1996; Volume 5.

15. Sartori, A. Avaliação Da Classificação Hidrológica Do Solo Para a Determinação Do Excesso de Chuva Do Método Do Serviço de Conservação Do Solo Dos Estados Unidos. Ph.D. Thesis, Faculty of Civil Engineering, Architecture and Urbanism, State University of Campinas, Campinas, Brazil, 2004.
16. Yu, K.; Pypker, T.G.; Keim, R.F.; Chen, N.; Yang, Y.; Guo, S.; Li, W.; Wang, G. Canopy Rainfall Storage Capacity as Affected by Sub-Alpine Grassland Degradation in the Qinghai–Tibetan Plateau, China. *Hydrol. Process.* **2012**, *26*, 3114–3123. https://doi.org/10.1002/hyp.8377.
17. Palmer, T.N.; Doblas-Reyes, F.J.; Hagedorn, R.; Weisheimer, A. Probabilistic Prediction of Climate Using Multi-Model Ensembles: From Basics to Applications. *Philos. Trans. R. Soc. B Biol. Sci.* **2005**, *360*, 1991–1998.
18. Sun, S.; Chen, H.; Ju, W.; Hua, W.; Yu, M.; Yin, Y. Assessing the Future Hydrological Cycle in the Xinjiang Basin, China, Using a Multi-Model Ensemble and SWAT Model. *Int. J. Climatol.* **2014**, *34*, 2972–2987. https://doi.org/10.1002/joc.3890.
19. Arnell, N.W.; Livermore, M.J.L.; Kovats, S.; Levy, P.E.; Nicholls, R.; Parry, M.L.; Gaffin, S.R. Climate and Socio-Economic Scenarios for Global-Scale Climate Change Impacts Assessments: Characterising the SRES Storylines. *Glob. Environ. Change* **2004**, *14*, 3–20. https://doi.org/10.1016/j.gloenvcha.2003.10.004.
20. Heo, J.-H.; Ahn, H.; Shin, J.-Y.; Kjeldsen, T.R.; Jeong, C. Probability Distributions for a Quantile Mapping Technique for a Bias Correction of Precipitation Data: A Case Study to Precipitation Data Under Climate Change. *Water* **2019**, *11*, 1475. https://doi.org/10.3390/w11071475.
21. Monteiro, J.A.F.; Kamali, B.; Srinivasan, R.; Abbaspour, K.; Gücker, B. Modelling the Effect of Riparian Vegetation Restoration on Sediment Transport in a Human-Impacted Brazilian Catchment: Modelling Riparian Restoration. *Ecohydrology* **2016**, *9*, 1289–1303. https://doi.org/10.1002/eco.1726.
22. Abbaspour, K.C.; Vaghefi, S.A.; Srinivasan, R. A Guideline for Successful Calibration and Uncertainty Analysis for Soil and Water Assessment: A Review of Papers from the 2016 International SWAT Conference. *Water* **2018**, *10*, 6. https://doi.org/10.3390/w10010006.
23. Abbaspour, K.C. *SWAT Calibration and Uncertainty Programs*; Eawag: Diebendorf, Switzerland, 2015; 100p.
24. Abbaspour, K.C.; Yang, J.; Maximov, I.; Siber, R.; Bogner, K.; Mieleitner, J.; Zobrist, J.; Srinivasan, R. Modelling Hydrology and Water Quality in the Pre-Alpine/Alpine Thur Watershed Using SWAT. *J. Hydrol.* **2007**, *333*, 413–430. https://doi.org/10.1016/j.jhydrol.2006.09.014.
25. Gupta, H.V.; Kling, H.; Yilmaz, K.K.; Martinez, G.F. Decomposition of the Mean Squared Error and NSE Performance Criteria: Implications for Improving Hydrological Modelling. *J. Hydrol.* **2009**, *377*, 80–91. https://doi.org/10.1016/j.jhydrol.2009.08.003.
26. Kouchi, D.H.; Esmaili, K.; Faridhosseini, A.; Sanaeinejad, S.H.; Khalili, D.; Abbaspour, K.C. Sensitivity of Calibrated Parameters and Water Resource Estimates on Different Objective Functions and Optimization Algorithms. *Water* **2017**, *9*, 384. https://doi.org/10.3390/w9060384.
27. Nash, J.E.; Sutcliffe, J.V. River Flow Forecasting through Conceptual Models Part I — A Discussion of Principles. *J. Hydrol.* **1970**, *10*, 282–290. https://doi.org/10.1016/0022-1694(70)90255-6.
28. Llorens, P.; Gallart, F. A Simplified Method for Forest Water Storage Capacity Measurement. *J. Hydrol.* **2000**, *240*, 131–144. https://doi.org/10.1016/S0022-1694(00)00339-5.
29. Putuhena, W.M.; Cordery, I. Estimation of Interception Capacity of the Forest Floor. *J. Hydrol.* **1996**, *180*, 283–299. https://doi.org/10.1016/0022-1694(95)02883-8.
30. Jackson, I.J. Relationships between Rainfall Parameters and Interception by Tropical Forest. *J. Hydrol.* **1975**, *24*, 215–238. https://doi.org/10.1016/0022-1694(75)90082-7.
31. Herwitz, S.R. Interception Storage Capacities of Tropical Rainforest Canopy Trees. *J. Hydrol.* **1985**, *77*, 237–252. https://doi.org/10.1016/0022-1694(85)90209-4.
32. Martins, L.L.; Martins, W.A.; de Moraes, J.F.L.; Júnior, M.J.P.; De Maria, I.C. Calibração Hidrológica Do Modelo SWAT Em Bacia Hidrográfica Caracterizada Pela Expansão Do Cultivo Da Cana-de-Açúcar. *Rev. Bras. Geogr. Física* **2020**, *13*, 576–594.
33. Moriasi, D.N.; Arnold, J.G.; van Liew, M.W.; Bingner, R.L.; Harmel, R.D.; Veith, T.L. Model Evaluation Guidelines for Systematic Quantification of Accuracy in Watershed Simulations. *Trans. ASABE* **2007**, *50*, 885–900. https://doi.org/10.13031/2013.23153.